Liquid Transport Through Nanoscale Porous Media with Strong Wettability

Jie Zhang[1] · **Hongqing Song**[1] · **Weiyao Zhu**[1] · **Jiulong Wang**[1]

Abstract

It is important to investigate interfacial effects on liquid transport characteristics through nanopores with strong wettability due to potential applications in several fields. The structural and transport properties of wetted liquid argon through nanochannels were investigated via molecular dynamics (MD) simulations. A mathematical model for liquid flow in nanoporous media was established based on the constant negative slip length by combining MD simulations with fractal theory for complex media. The results show that the strong liquid–solid attraction allows the liquid to be adsorbed onto the solid walls. In addition, compared with the bulk diffusion coefficient in the center of the nanochannel, the coefficient parallel to the interface near the solid walls is largely reduced, indicating the liquid molecules are strongly bound to the solid walls. Furthermore, negative slip can exist in the vicinity of solid walls with strong wettabilities. The variations in negative slip length with the external driving force can be characterized by two regimes. In steady negative slip regime, the negative slip length remains constant. As the driving force continues to increase, the transition negative slip regime exists, where the negative slip length decreases linearly with the driving force until the slip length becomes zero. The presence of a negative slip length reduces the liquid flow rate compared with no slip or a positive slip length due to the reduced effective cross section for fluid transport. Moreover, the increased fractal dimensions about the capillary radius result in an enhanced liquid flow rate, while that about the tortuosity reduces the liquid flow rate.

Keywords Interfacial effects · Slip length · Nanoscale porous media · Fractal theory

1 Introduction

Understanding the interfacial effects on liquid transport behavior, especially on the slip flow behavior through nanoscale porous media, has several important applications in various fields, such as the design of nanofluidic devices (Ewen et al. 2018), water purification (Shannon et al. 2010), nanomedicine applications (Ababaei and Abbaszadeh 2017;

✉ Hongqing Song
  songhongqing@ustb.edu.cn

[1] School of Civil and Resource Engineering, University of Science and Technology Beijing, Beijing 100083, China

Esmaeili et al. 2020), and geological resource development (Wang et al. 2019; Zhang et al. 2014). For example, in unconventional reservoir development, such as the recovery of shale oil and gas, the relatively small pore sizes generally restrict liquid flow to microscale or even nanoscale spaces (Letham and Bustin 2018; Song et al. 2015; Wang and Sheng 2017; Wei et al. 2018). In this case, the process of wetting a solid surface with a liquid gives a much stronger attraction between the liquid and solid wall compared with macroscale liquid flow. As a result, the structural and transport properties of nanoscale liquids differ significantly from bulk liquids. In particular, the traditional no-slip boundary condition may break down in this scenario, and it is inaccurate to apply the classical Hagen–Poiseuille equation to the predicted liquid flow rates. It has been reported that the liquid slippage near the solid surfaces could enhance the liquid flow rate compared with that of no-slip boundary condition (Secchi et al. 2016; Thomas and McGaughey 2009). Therefore, the interfacial effects, such as from a strong wettability, should be considered to investigate the liquid boundary slip and transport characteristics in nanoporous media.

In recent years, many scholars have studied when and why no-slip boundary conditions become invalid for flow systems at the nanoscale. It was shown that the downsizing led to an increased surface to volume ratio, where the influence of the interfacial properties on liquid transport was predominant. For example, Myers proposed a mathematical model that consists of a depletion layer with reduced viscosity near the solid wall and a bulk flow region. He found that as the radius of the carbon nanotubes decreased, the flow enhancement increased, and in the limit of large tubes, there was no noticeable flow enhancement (Myers 2011). Secchi et al. (2016) measured the water slippage in various nanotubes and showed that the water slippage is large and radius-dependent in carbon nanotubes, but there is no slippage in boron nitride nanotubes due to their different electronic structures. Furthermore, continuous progress has been made toward investigating the slip length, which reflects the amount of slip at a given surface, using experiments and computer simulations. It has been demonstrated that the slip length depends upon several different factors, including the surface wettability (Cieplak et al. 2001; Cottin-Bizonne et al. 2008; Huang et al. 2008; Xue et al. 2014), shear rate (flow rate) (Craig et al. 2001; Thompson and Troian 1997; Zhu and Granick 2001), surface roughness (Bonaccurso et al. 2003; Kumar et al. 2016; Pit et al. 2000; Yang 2006), surface energy corrugation (Tocci et al. 2014), nanotube radius (Secchi et al. 2016), properties of the confined liquid (density (Cieplak et al. 2001), viscosity, and polarity (Cho et al. 2004)), and depletion layer thickness (Sendner et al. 2009). Xue et al. (2014) investigated the influence of the solid–liquid adhesive properties on liquid slippage at solid surfaces. They proposed a theoretical model that directly relates the liquid slip length to the liquid adhesive force on solid surfaces. Huang et al. (2008) studied the interfacial slippage of water at various hydrophobic surfaces. They found a quasi-universal relationship between the water slippage and contact angle. Tocci et al. (2014) compared the flow behavior of liquid water on graphene with that on hexagonal boron nitride. They found that while both water–solid interfaces showed similar structures, the slippages were quite different due to differences in the surface energy corrugations of the two sheets. Luan and Zhou studied the wettability and friction of water on a MoS_2 nanosheet and found that the MoS_2 nanosheet presented the typical hydrophobicity with low friction coefficient (or large slip length) (Luan and Zhou 2016).

Apart from the aforementioned works which focused on the variations in the positive slip length, there are also some works which investigated negative slip in nanochannels or nanopores (Cieplak et al. 2001, 2006; Gruener et al. 2009, 2016; Sendner et al. 2009; Wang et al. 2016a, b; Yang 2006; Zhan et al. 2020). As shown in Fig. 1, compared with a positive slip where liquid slides at solid surfaces, the negative slip length is defined as the

Fig. 1 Schematic representation of different flow characteristics in nanotubes. (a) Positive slip flow occurs near the solid wall where v_s is the slip velocity and b is the positive slip length; (b) classical no-slip flow occurs near the solid wall; and (c) static thin liquid film exists near the solid wall where b_0 is the negative slip length
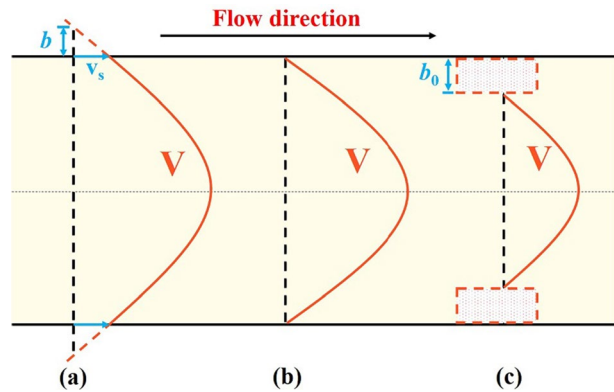
thickness of the immobile liquid layer in the vicinity of a solid surface (Pottier et al. 2015). The presence of this immobile liquid layer is due to a strong attraction to the solid surface, which inevitably affects the transport properties of liquids, especially when confined to the nanoscale. However, most of the previous reports did not integrate the negative slip length into mathematical models for liquid transport in nanoporous media. Moreover, they also did not study the variations in the negative slip length with its influencing factors. Therefore, it is important to further investigate the effects of the negative slip length on the liquid transport behavior when the solid walls are strongly wetted by a liquid in nanosized flow systems.

This paper considered three aspects of nanoscale liquid flow. First, the structural and transport properties of liquid argon through a nanochannel with a strong wettability were investigated via molecular dynamics (MD) simulations. Second, the fractal theory of complex media was combined with the MD simulation results and a mathematical model for single-phase fluid flow in nanoporous media was established. Third, analyses of the negative slip length and fractal dimension were performed to determine their relationships with the liquid flow rate in nanoscale porous media. These results can be widely applied in many areas related to nanohydrodynamics in porous media.

2 Methodology

2.1 Molecular Dynamics Simulations

To investigate the structural and transport properties of fluid through nanochannels, we performed MD simulations using the open-source package LAMMPS (Plimpton 1995). As shown in Fig. 2, two parallel walls were considered in the x–y plane where each consisted of six layers of gold molecules arranged in an face-centered cubic (fcc) lattice where its (100) surface was in contact with liquid argon molecules. The distance h between two walls was 6.1 nm. Periodic boundary conditions were imposed along the x and y directions. We employed the Lennard–Jones (LJ) potential to model the liquid–liquid interactions as $V_{\mathrm{LJ}}(r) = 4\varepsilon\left[\left(\frac{\sigma}{r}\right)^{12} - \left(\frac{\sigma}{r}\right)^{6}\right]$. Here, r is the interatomic separation, σ is the size of the repulsive core, and ε is the depth of the potential well. The wall molecules were fixed at their initial locations and did not include wall–wall molecular interactions. The parameters

Fig. 2 Schematic and dimensions of the simulation system
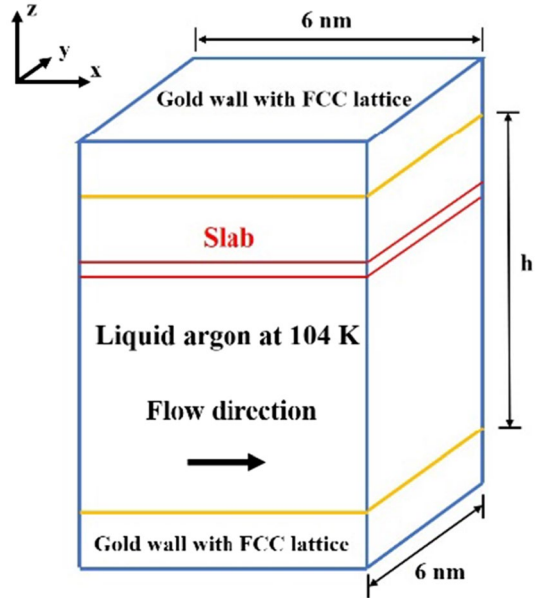
used to model the molecular interactions for argon and gold molecules were $\sigma_{Ar} = 0.3405$ nm, $\varepsilon_{Ar} = 1.65399 \times 10^{-21}$ J, $\sigma_{Au} = 0.2934$ nm, and $\varepsilon_{Au} = 2.7096 \times 10^{-22}$ J (Ghorbanian and Beskok 2016). These potential parameters were shown to reproduce the thermodynamics properties and flow characteristics of liquid argon at the nanoscale pretty well.

For wall–liquid interactions, we used the modified LJ potential as $V_{wl}(r) = 4\varepsilon_{wl}\left[\left(\frac{\sigma_{wl}}{r}\right)^{12} - \beta\left(\frac{\sigma_{wl}}{r}\right)^{6}\right]$. Here, $\sigma_{wl} = (\sigma_{Ar} + \sigma_{Au})/2$ and the depth of the potential well $\varepsilon_{wl} = \alpha \cdot \sqrt{\varepsilon_{Ar} \cdot \varepsilon_{Au}}$ were determined based on the Lorentz–Berthelot combination rule (Delhommelle and Millié 2001; Yezdimer et al. 2001). The parameter α is the potential energy factor that indicates the attractive strength between molecules and β is the potential energy factor that indicates the repulsive strength. As shown in the work by Nagayama and Cheng, $\beta = 1$ represented the zero contact angle, that is, the solid surface was completely wetted by the liquid. In addition, the increasing values of α led to the increasing strength of hydrophilic interactions (Nagayama and Cheng 2004). In this study, we took the values $\alpha = 3.5$ and $\beta = 1$ to simulate the wetting of the solid surface due to the liquid. To reduce the computational costs, the LJ potential was truncated at a distance of $3.2\sigma_{Ar}$. The temperature and pressure of the system were maintained at 104 K and 1.5 MPa, respectively, under which condition, the desired density of liquid argon was 1291.1 kg/m^3.

At the beginning of the simulations, the system was allowed to equilibrate using canonical NVT ensemble, and the simulation time for this equilibration period was 2 ns at a time step of 1 fs. Then, a constant body force in the stream-wise direction was added to each liquid molecule for the non-equilibrium MD simulations. The acceleration of each liquid argon molecule induced by the body force was maintained on the order of 10^{-4}–10^{-3} nm/ps^2, which ensures a linear system response (Falk et al. 2012). In order to reach the steady state, each case for different driving forces was run for 20 ns. After reaching steady state, the simulations were extended over 25 ns, during which the results were recorded every

25×10^3 time steps. Therefore, 1000 data sets were obtained to perform time averaging. The spatial averaging for the density profile was performed in slabs with a thickness of 0.03 nm parallel to the z axis. However, the thickness of a single slab was 0.3 nm for the velocity profile.

2.2 Fractal Theory of Complex Media

Previous studies have shown that fractal geometry theory can be utilized to accurately characterize the geometrical structures of media with nanoscale pores (Ghanbarian et al. 2016; Wang et al. 2019; Yang et al. 2015). The key point to establish the fractal characterization model is to determine the fractal dimensions. For a typical fractal model with slits, assuming that the slit widths are λ and distributed continuously from $\lambda_{\min}$ to $\lambda_{\max}$ on a per unit area of the cross section, the cumulative number N_c of slits with widths greater than λ is

$$N_c(\lambda) = \left(\frac{\lambda_{\max}}{\lambda} \right)^{D_p} \tag{1}$$

where D_p is the fractal dimension about the slit width. After differentiating Eq. 1 with respect to λ, the number of slits with widths between λ and $\lambda + d\lambda$ can be obtained as

$$-dN_c = D_P \cdot \lambda_{\max}^{D_p} \cdot \lambda^{-(1+D_p)} d\lambda \tag{2}$$

Moreover, the actual flow path is nonlinear for fluid flow through fractal porous media. Thus, the fluid particles always travel further than the straight-line distance would indicate. A scaling law between the actual flow path L_a and the apparent flow path L was proposed by Wheatcraft as (Wheatcraft and Tyler 1988)

$$L_a(\lambda) = \lambda^{1-D_T} \cdot L^{D_T} \tag{3}$$

where D_T is the fractal dimension about the tortuosity.

The procedures to incorporate fractal theory into an established mathematical model for single-phase fluid flow in porous media is summarized as follows. First, nuclear magnetic resonance (NMR) analyses were performed for typical shale reservoir cores to obtain the pore size distributions. Second, the pore size distributions were used to determine the fractal dimensions and other parameters to establish the fractal pore characterization model. Third, the flow rate equation for single pipe fluid flow was used with the fractal pore characterization model to establish a mathematical model for single-phase fluid flow in porous media.

2.3 Calculation Process

The calculation process is shown in Fig. 3. First, we performed MD simulations to study the structural and transport properties of liquid argon through nanochannels with a strong wettability. Second, the MD results were used with fractal theory to establish a mathematical model and calculate the liquid flow rate in nanoporous media. Third, the effects of the negative slip length and fractal dimension of the nanoporous media on the liquid flow rate through it were investigated.

Fig. 3 Workflow to investigate
the liquid transport properties in
nanoporous media with a strong
wettability
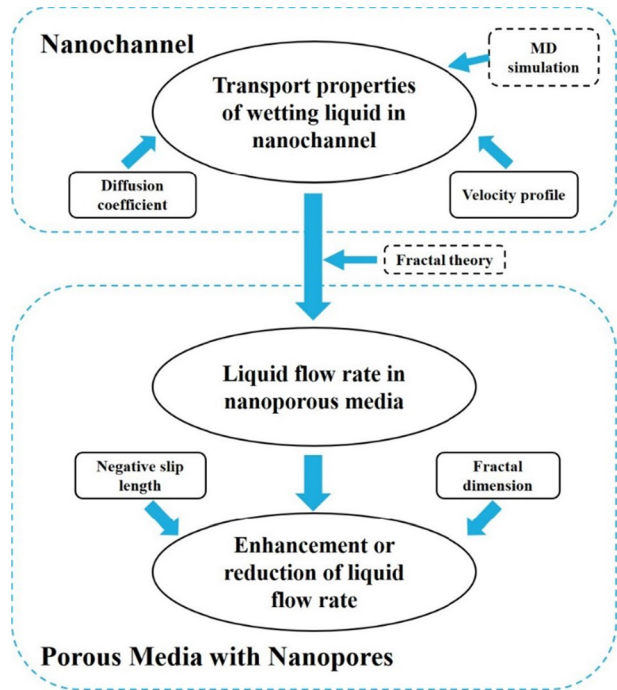
3 Results and Discussion

Before the discussion part, the physical model for the molecular dynamics simulation
was verified in terms of bulk density and self-diffusion coefficient of liquid argon, as
shown in Sects. 3.1 and 3.2.

3.1 Density Profiles in Nanochannel

First, the density distribution of liquid argon between two solid walls with a strong
wettability was examined to provide insight into the liquid structure in the vicinity of
the interface. As shown in Fig. 4, the density profile was symmetric across the chan-
nel height, and the liquid argon density showed strong oscillations near the solid walls.
These oscillations indicate the pronounced density layering effects of liquid argon,
which were induced by the adsorption of liquid molecules onto the solid walls.

Further from the solid walls, the density oscillations were gradually suppressed and
the density of the liquid argon stabilized to a value, which is in agreement with the
desired value at 104 K and 1.5 MPa. We compared the density profiles of liquid argon
under different driving forces to further investigate their effects on the density distribu-
tions. The four curves from the different driving forces nearly overlap each other for all
of liquid film heights, which agrees with several previous reports (Wang et al. 2016a, b;
Yang 2006). This indicates that the density structures of nanoconfined liquids are inde-
pendent of the driving force but are significantly affected by the liquid–solid interface
properties.
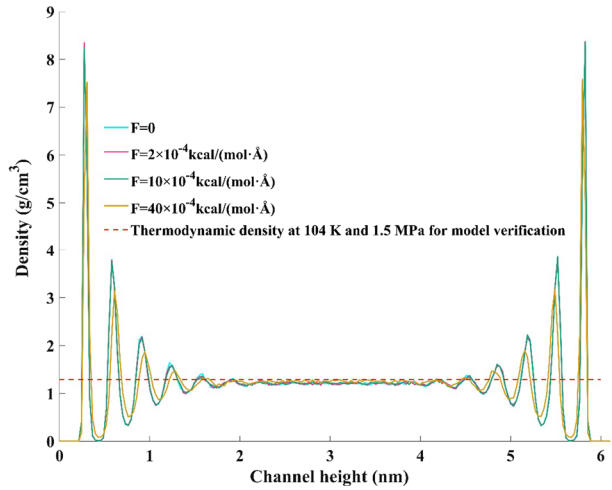
3.2 Self-diffusion Coefficient in Nanochannel

The diffusion coefficient can reflect the ability of liquid molecules to spontaneously migrate into the same or different species. For homogeneous systems, such as bulk liquids, the Einstein or Green–Kubo relation is generally utilized to calculate the diffusion coefficient. Liu et al. proposed a mathematical model that modified the Einstein relation to calculate the diffusion coefficient of heterogeneous systems, which is applicable when investigating diffusion problems near interfaces (Chilukoti et al. 2014; Liu et al. 2004). Here, the spatial distribution of the parallel diffusion coefficient along the channel height was investigated using this model. The parallel diffusion coefficient is calculated as (Chilukoti et al. 2014)

$$D_{xx}(i) = \lim_{\tau \to \infty} \frac{\left\langle \Delta x(\tau)^2 \right\rangle_i}{2\tau S(\tau)} \tag{4}$$

where $D_{xx}(i)$ is the diffusion coefficient along the x direction of slab i, and $\left\langle \Delta x(\tau)^2 \right\rangle_i$ denotes the ensemble average of the mean square displacement (MSD) along the x direction of the molecules that are continuously in slab i during the time period τ as calculated using (Chilukoti et al. 2014)

$$\left\langle \Delta x(\tau)^2 \right\rangle_i = \frac{1}{N(0)} \cdot \sum_{j \in i} (x_j(\tau) - x_j(0))^2 \tag{5}$$

where $N(0)$ is the initial number of the molecules at a given time in slab i, and $S(\tau)$ is the survival probability defined as $S(\tau) = N(0, \tau)/N(0)$, where $N(0, \tau)$ is the number of molecules that are continuously present at time τ.

Figure 5a shows the division of slabs for only half the channel height due to symmetry. To contain the adsorption layer in a single slab, the thickness of the slab nearest the solid wall was determined based on the distance of two consecutive density oscillation valleys. Figure 5b shows the variations in the survival probability with time. It is seen that except for slab 1, the survival probability of nearly all slabs decreased with time due to the diffusive nature of liquid molecules. For slab 1, which is nearest the solid wall, the attraction of the wall to the liquid was the strongest and the liquid molecules remained in this slab over

Fig. 5 For liquid argon near the gold (100) surface, (a) the division of slabs for half the channel height based on the density profile; (b) variations in the survival probability with time for different slabs; and (c) variations of the mean square displacement (MSD) in the x direction with time for different slabs


(a)

(b)

(c)
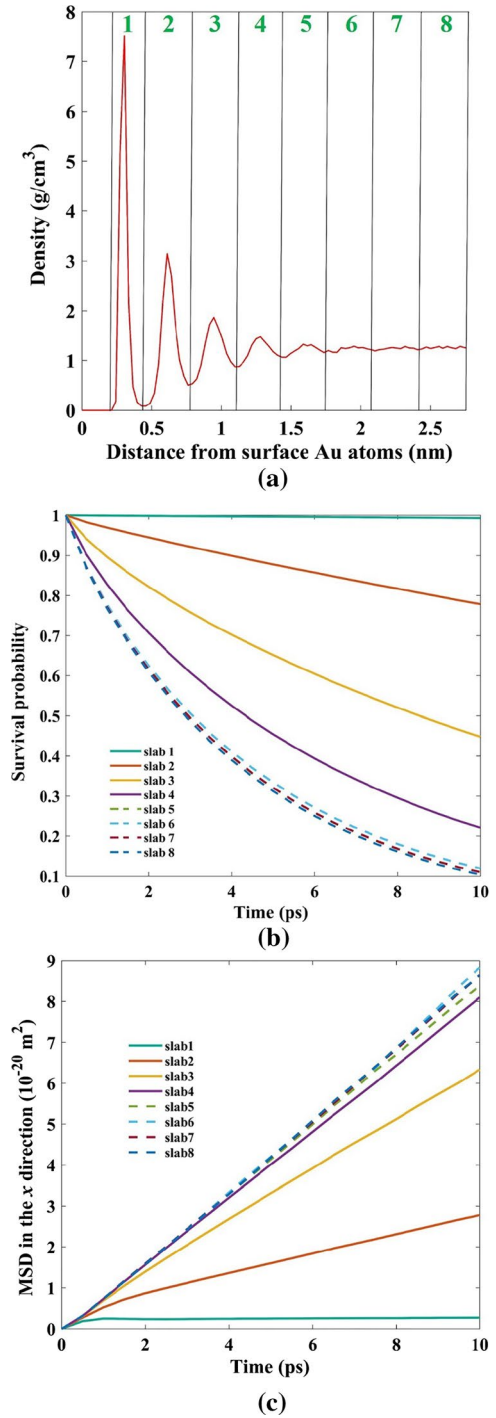
the entire time interval. Figure 5c shows the variations of the MSD along the x direction with time for different slabs. The slope of the MSD versus time represents the diffusivity of liquid molecules, which clearly shows that the diffusion coefficients in the bulk region differed significantly from that in the interface region.

The calculated diffusion coefficients D_{xx} for different slabs are shown in Fig. 6. It is observed that the parallel diffusion coefficient reduced when the liquid was close to the interface. Away from the interface, the bulk diffusion coefficient recovered with an average value of 4.5×10^{-9} m²/s at 104 K, in agreement with the simulation results in Lee et al. (2003), which is $(2.48 \pm 0.07) \times 10^{-9}$ m²/s at 94.4 K. It is noted that at slab 1, the diffusion coefficient was nearly zero, which indicates the liquid argon molecules were strongly bound to the solid wall.

3.3 Velocity Profiles and Negative Slip Length

The velocity profiles for liquid argon flow through the gold nanochannel with a strong wettability under two different driving forces are shown in Fig. 7. It is observed that both velocity profiles exhibit parabolic shapes; with an increasing driving force, the maximum velocity also increased. In addition, Fig. 7a shows that there exists a static thin liquid film near the solid walls, which indicates the presence of a negative slip length. In our case, the negative slip length is approximately -0.53 nm, which agrees with the results in Sendner et al. (2009). Meanwhile, it is noted that the negative slip length is not a constant and depends on several factors, such as the surface wettability (Cieplak et al. 2001) and the driving force (Yang 2006). Figure 8 shows the variation of negative slip length with the external driving force. As shown in Fig. 8, there are two regimes for the variation of negative slip length with the external driving force. The first regime is called steady negative slip regime (SNSR), that is, the negative slip length remains constant in this regime. It is the maximum negative slip length reflecting the maximum number of immobile adsorbing fluid layers in the vicinity of solid wall. When continuously increasing the driving force, the second regime, which is called transition negative slip regime (TNSR), exists and can characterize the variation of negative slip length. With the increase in driving force, the

Fig. 6 Diffusion coefficient D_{xx} for liquid argon as a function of distance from the solid wall. The dashed line represents the bulk diffusion coefficient
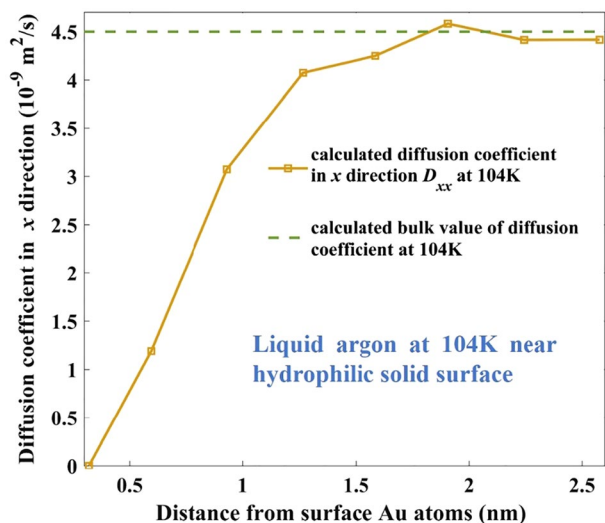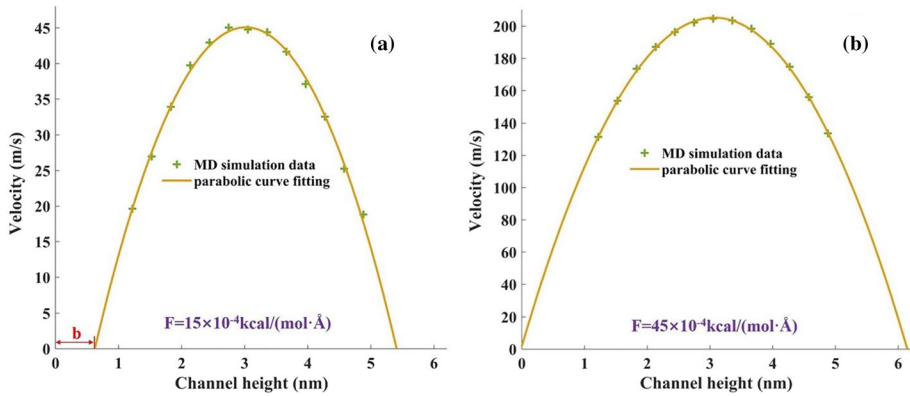
Fig. 7 Velocity profiles for liquid argon flow in the nanochannel for two different driving forces. **a** Driving force of $F = 15 \times 10^{-4}$ kcal/(mol Å) where b is the negative slip length, and **b** driving force of $F = 45 \times 10^{-4}$ kcal/(mol Å)

Fig. 8 Variations in negative slip length with external driving force. The green circles correspond to the MD simulation results, and the uncertainty comes from the noise of data points. The yellow line is a guide to the eye
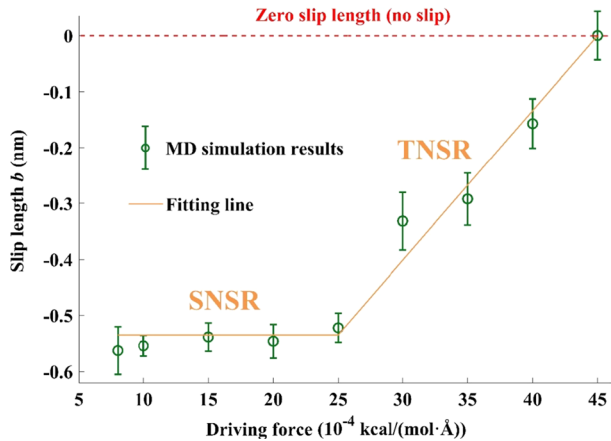
negative slip length linearly decreases until the slip length becomes zero. In this regime, the adsorbing fluid layer with less attraction by the solid wall, that is, relatively away from solid wall, starts to slide along adjacent fluid layers. When increasing the driving force, more and more adsorbing fluid layers begin moving, indicating the less thickness of immobile layers.

3.4 Flow Rate in Nanoporous Media

A cylindrical nanoporous medium with height h and radius R is considered. It is assumed that the medium can be characterized using a fractal geometry model with a series of capillaries where the liquid flows along the radial direction. Combining fractal theory with a constant negative slip length gives a mathematical model to calculate the liquid flow rate through nanoporous media as

$$Q = \frac{dP}{dR} \cdot \frac{\pi^2 \cdot h \cdot R^{2-D_T} \cdot D_P \cdot \lambda_{\max}^{D_P}}{4\mu D_T} \cdot \int_{\lambda_{\min}}^{\lambda_{\max}} (\lambda - b_0)^4 \cdot \lambda^{D_T - D_P - 2} d\lambda \qquad (6)$$

where $\frac{dP}{dR}$ is the pressure gradient, D_P and D_T are the fractal dimensions about the capillary radius and tortuosity, respectively, $\lambda_{\max}$ and $\lambda_{\min}$ are the maximum and minimum capillary radii, respectively, b_0 is the constant negative slip length, and μ is the liquid viscosity. It is seen from Eq. 6 that while the liquid flow rate is proportional to the pressure gradient, the presence of a negative slip length affects the slope of the linear line. When b_0 is zero, Eq. 6 reduces to the classical equation for liquid flow with a no-slip boundary condition through porous media.

Figure 9 shows the variations in the liquid flow rate with the pressure gradient for different slip length magnitudes. It is observed that the negative slip length reduced the liquid flow rate compared with the cases of no slip and positive slip lengths under the same pressure gradient. Meanwhile, the increased magnitude of the negative slip length also increased the reduction in the flow rate. As reported by Pottier (Pottier et al. 2015), the immobile layer close to the wall behaves as a solid-like layer, and its properties differ significantly from the bulk liquid. In effect, the existence of this solid-like layer causes the wall to thicken. As a result, the effective cross section for fluid transport is reduced due to the narrowed pore space, which leads to a decreased liquid flow rate. In addition, Fig. 9 shows that compared with the case of no slip, the constant positive slip length led to an enhanced liquid flow rate, which agrees with the previous reports (Secchi et al. 2016; Thomas and McGaughey 2009).

3.5 Effects of Fractal Dimensions in Nanoporous Media

The effects of the geometrical structure of a nanoporous media on the liquid flow rate are further investigated with focus on the fractal dimensions. Figure 10a shows the variations in the liquid flow rate through nanoporous media with the pressure gradient for different fractal dimensions about the capillary radius. The figure shows that an increased D_P resulted in

Fig. 9 Variations in the liquid flow rate through nanoporous media with the pressure gradient for different slip length magnitudes
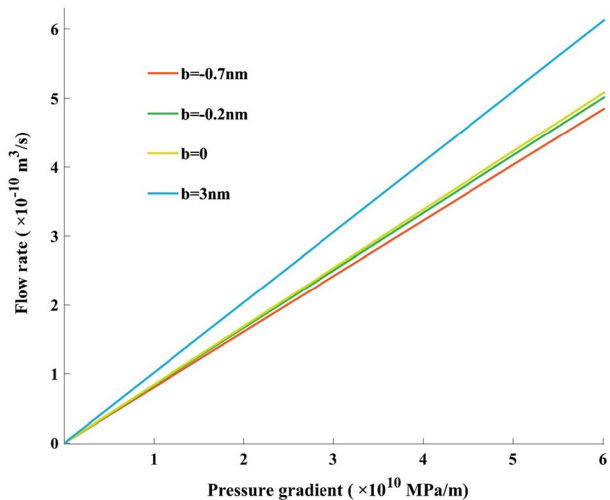
Fig. 10 Variations in the liquid flow rate through nanoporous media with the pressure gradient for different fractal dimensions about the **a** capillary radius D_P and **b** tortuosity D_T
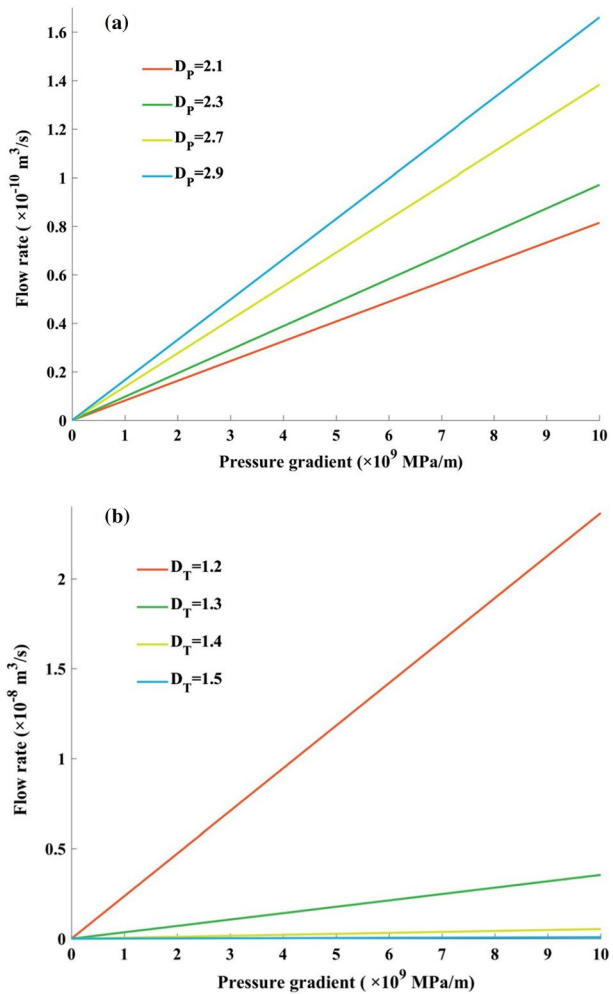
an enhanced liquid flow rate. As D_P increases, the number of capillaries per unit area of the cross section for the fractal model correspondingly increases, which implies a more developed fracture network or more connected pores for the typical media. A porous media with more connected pores favors liquid transport, resulting in an increased overall flow rate. Figure 10b shows the variations in the liquid flow rate through nanoporous media with the pressure gradient for different fractal dimensions about the tortuosity. The figure shows that as D_T increased, the liquid flow rate decreased under the same pressure gradient. A larger D_T indicates more bending streamlines for the liquid flow. As a result, the energy dissipation in the vicinity of the solid walls increases, which reduces the liquid flow rate through medium.

4 Conclusions

Understanding the interfacial effects on liquid transport behavior through nanopores with strong wettability plays an important role in several areas, including the design of nanofluidic devices and the development of unconventional reservoirs. The structural and transport properties of wetted liquid argon through a nanochannel were first investigated through MD simulations. Then, a mathematical model for liquid flow in nanoporous media was established based on the MD results as combined with fractal theory for complex media. Finally, an analysis of the negative slip length and the fractal dimension was performed to determine its relationship with the liquid flow rate for nanoscale porous media.

The results show that liquid can be adsorbed onto the gold solid walls due to a strong liquid–solid attraction. The diffusion coefficient parallel to the wall-liquid interface was reduced near the solid walls as compared with the bulk value in the middle of the nanochannel. In addition, a negative slip length can exist near the solid surface with a strong wettability, and its magnitude varied with external driving force. The variations in negative slip length with the driving force can be characterized by two regimes. In steady negative slip regime, the negative slip length is a constant and independent of the driving force. With the continuous increase in the driving force, the transition negative slip regime exists, where the negative slip length decreased linearly with the driving force until the slip length became zero.

Combined with fractal theory, a mathematical model to calculate the liquid flow rate in nanoporous media was established based on the constant negative slip length. Due to reduced effective cross section for fluid transport from the presence of a negative slip length, the liquid flow rate is reduced compared with the cases of no slip or a positive slip length. Moreover, the increased fractal dimensions about the capillary radius resulted in an enhanced liquid flow rate, while an increased fractal dimension about the tortuosity led to a reduced liquid flow rate as more energy was dissipated. Investigating the negative slip phenomenon is of great value owing to many potential applications, such as unconventional oil/gas development and fabrication of nanofluidic devices. For future work, the applicability of variation in negative slip length with external driving force and other factors should be further validated on other Newtonian fluids with properties like polarity.

References

Ababaei, A., Abbaszadeh, M.: Second law analyses of forced convection of low-Reynolds-number slip flow of nanofluid inside a microchannel with square impediments. Glob. J. Nanomed. **1**, 4 (2017)

Bonaccurso, E., Butt, H.-J., Craig, V.S.: Surface roughness and hydrodynamic boundary slip of a Newtonian fluid in a completely wetting system. Phys. Rev. Lett. **90**, 144501 (2003)

Chilukoti, H.K., Kikugawa, G., Ohara, T.: Structure and transport properties of liquid alkanes in the vicinity of α-quartz surfaces. Int. J. Heat Mass Transf. **79**, 846–857 (2014)

Cho, J.-H.J., Law, B.M., Rieutord, F.: Dipole-dependent slip of Newtonian liquids at smooth solid hydrophobic surfaces. Phys. Rev. Lett. **92**, 166102 (2004)

Cieplak, M., Koplik, J., Banavar, J.R.: Boundary conditions at a fluid–solid interface. Phys. Rev. Lett. **86**, 803 (2001)

Cieplak, M., Koplik, J., Banavar, J.R.: Nanoscale fluid flows in the vicinity of patterned surfaces. Phys. Rev. Lett. **96**, 114502 (2006)

Cottin-Bizonne, C., Steinberger, A., Cross, B., Raccurt, O., Charlaix, E.: Nanohydrodynamics: the intrinsic flow boundary condition on smooth surfaces. Langmuir **24**, 1165–1172 (2008)

Craig, V.S., Neto, C., Williams, D.R.: Shear-dependent boundary slip in an aqueous Newtonian liquid. Phys. Rev. Lett. **87**, 054504 (2001)

Delhommelle, J., Millié, P.: Inadequacy of the Lorentz-Berthelot combining rules for accurate predictions of equilibrium properties by molecular simulation. Mol. Phys. **99**, 619–625 (2001)

Esmaeili, A.R., Sajadi, B., Akbarzadeh, M.: Numerical simulation of ellipsoidal particles deposition in the human nasal cavity under cyclic inspiratory flow. J. Braz. Soc. Mech. Sci. **42**, 243 (2020)

Ewen, J.P., Kannam, S.K., Todd, B., Dini, D.: Slip of alkanes confined between surfactant monolayers adsorbed on solid surfaces. Langmuir **34**, 3864–3873 (2018)

Falk, K., Sedlmeier, F., Joly, L., Netz, R.R., Bocquet, L.: Ultralow liquid/solid friction in carbon nanotubes: comprehensive theory for alcohols, alkanes, OMCTS, and water. Langmuir **28**, 14261–14272 (2012)

Ghanbarian, B., Hunt, A.G., Daigle, H.: Fluid flow in porous media with rough pore-solid interface. Water Resour. Res. **52**, 2045–2058 (2016)

Ghorbanian, J., Beskok, A.: Scale effects in nano-channel liquid flows. Microfluid. Nanofluid. **20**, 121 (2016)

Gruener, S., Hofmann, T., Wallacher, D., Kityk, A.V., Huber, P.: Capillary rise of water in hydrophilic nanopores. Phys. Rev. E **79**, 067301 (2009)

Gruener, S., Wallacher, D., Greulich, S., Busch, M., Huber, P.: Hydraulic transport across hydrophilic and hydrophobic nanopores: flow experiments with water and *n*-hexane. Phys. Rev. E **93**, 013102 (2016)

Huang, D.M., Sendner, C., Horinek, D., Netz, R.R., Bocquet, L.: Water slippage versus contact angle: a quasiuniversal relationship. Phys. Rev. Lett. **101**, 226101 (2008)

Kumar, A., Datta, S., Kalyanasundaram, D.: Permeability and effective slip in confined flows transverse to wall slippage patterns. Phys. Fluids **28**, 082002 (2016)

Lee, S.-H., Park, D.-K., Kang, D.-B.: Molecular dynamics simulations for transport coefficients of liquid argon: new approaches. Bull. Korean Chem. Soc. **24**, 178–182 (2003)

Letham, E.A., Bustin, R.M.: Investigating multiphase flow phenomena in fine-grained reservoir rocks: insights from using ethane permeability measurements over a range of pore pressures. Geofluids **2018**, 1–13 (2018)

Liu, P., Harder, E., Berne, B.: On the calculation of diffusion coefficients in confined fluids and interfaces with an application to the liquid–vapor interface of water. J. Phys. Chem. B **108**, 6595–6602 (2004)

Luan, B., Zhou, R.: Wettability and friction of water on a MoS2 nanosheet. Appl. Phys. Lett. **108**, 131601 (2016)

Myers, T.G.: Why are slip lengths so large in carbon nanotubes? Microfluid. Nanofluid. **10**, 1141–1145 (2011)

Nagayama, G., Cheng, P.: Effects of interface wettability on microscale flow by molecular dynamics simulation. Int. J. Heat Mass Transf. **47**, 501–513 (2004)

Pit, R., Hervet, H., Leger, L.: Direct experimental evidence of slip in hexadecane: solid interfaces. Phys. Rev. Lett. **85**, 980 (2000)

Plimpton, S.: Fast parallel algorithms for short-range molecular dynamics. J. Comput. Phys. **117**, 1–19 (1995)

Pottier, B., Frétigny, C., Talini, L.: Boundary condition in liquid thin films revealed through the thermal fluctuations of their free surfaces. Phys. Rev. Lett. **114**, 227801 (2015)

Secchi, E., Marbach, S., Niguès, A., Stein, D., Siria, A., Bocquet, L.: Massive radius-dependent flow slippage in carbon nanotubes. Nature **537**, 210 (2016)

Sendner, C., Horinek, D., Bocquet, L., Netz, R.R.: Interfacial water at hydrophobic and hydrophilic surfaces: slip, viscosity, and diffusion. Langmuir **25**, 10768–10781 (2009)

Shannon, M.A., Bohn, P.W., Elimelech, M., Georgiadis, J.G., Marinas, B.J., Mayes, A.M.: Science and technology for water purification in the coming decades. In: Nanoscience and Technology: A Collection of Reviews from Nature Journals, pp. 337–346. World Scientific (2010)

Song, H., Yu, M., Zhu, W., Wu, P., Lou, Y., Wang, Y., Killough, J.: Numerical investigation of gas flow rate in shale gas reservoirs with nanoporous media. Int. J. Heat Mass Transf. **80**, 626–635 (2015)

Thomas, J.A., McGaughey, A.J.: Water flow in carbon nanotubes: transition to subcontinuum transport. Phys. Rev. Lett. **102**, 184502 (2009)

Thompson, P.A., Troian, S.M.: A general boundary condition for liquid flow at solid surfaces. Nature **389**, 360 (1997)

Tocci, G., Joly, L., Michaelides, A.: Friction of water on graphene and hexagonal boron nitride from ab initio methods: very different slippage despite very similar interface structures. Nano Lett. **14**, 6872–6877 (2014)

Wang, X., Sheng, J.J.: Understanding oil and gas flow mechanisms in shale reservoirs using SLD–PR transport model. Transport Porous Med. **119**, 337–350 (2017)

Wang, S., Feng, Q., Javadpour, F., Yang, Y.B.: Breakdown of fast mass transport of methane through calcite nanopores. J. Phys. Chem. C **120**, 14260–14269 (2016a)

Wang, S., Javadpour, F., Feng, Q.: Molecular dynamics simulations of oil transport through inorganic nanopores in shale. Fuel **171**, 74–86 (2016b)

Wang, J., Song, H., Rasouli, V., Killough, J.: An integrated approach for gas–water relative permeability determination in nanoscale porous media. J. Pet. Sci. Eng. **173**, 237–245 (2019)

Wei, M., Liu, J., Elsworth, D., Wang, E.: Triple-porosity modelling for the simulation of multiscale flow mechanisms in shale reservoirs. Geofluids **2018**, 1–11 (2018)

Wheatcraft, S.W., Tyler, S.W.: An explanation of scale-dependent dispersivity in heterogeneous aquifers using concepts of fractal geometry. Water Resour. Res. **24**, 566–578 (1988)

Xue, Y., Wu, Y., Pei, X., Duan, H., Xue, Q., Zhou, F.: How solid–liquid adhesive property regulates liquid slippage on solid surfaces? Langmuir **31**, 226–232 (2014)

Yang, S.-C.: Effects of surface roughness and interface wettability on nanoscale flow in a nanochannel. Microfluid. Nanofluid. **2**, 501–511 (2006)

Yang, S., Liang, M., Yu, B., Zou, M.: Permeability model for fractal porous media with rough surfaces. Microfluid. Nanofluid. **18**, 1085–1093 (2015)

Yezdimer, E.M., Chialvo, A.A., Cummings, P.T.: Examination of chain length effects on the solubility of alkanes in near-critical and supercritical aqueous solutions. J. Phys. Chem. B **105**, 841–847 (2001)

Zhan, S., Su, Y., Jin, Z., Wang, W., Cai, M., Li, L., Hao, Y.: Molecular insight into the boundary conditions of water flow in clay nanopores. J. Mol. Liq. **311**, 113292 (2020)

Zhang, X., Xiao, L., Shan, X., Guo, L.: Lattice Boltzmann simulation of shale gas transport in organic nanopores. Sci. Rep. **4**, 4843 (2014)

Zhu, Y., Granick, S.: Rate-dependent slip of Newtonian liquid at smooth surfaces. Phys. Rev. Lett. **87**, 096105 (2001)